We are IntechOpen,
the world's leading publisher of
Open Access books
Built by scientists, for scientists

6,900
Open access books available

186,000
International authors and editors

200M
Downloads

154
Countries delivered to

Our authors are among the

TOP 1%
most cited scientists

12.2%
Contributors from top 500 universities

CLARIVATE ANALYTICS

BOOK CITATION INDEX

INDEXED

WEB OF SCIENCE™

Selection of our books indexed in the Book Citation Index
in Web of Science™ Core Collection (BKCI)

Interested in publishing with us?
Contact book.department@intechopen.com

Numbers displayed above are based on latest data collected.
For more information visit www.intechopen.com

Methods for Wheel Slip and Sinkage Estimation in Mobile Robots

Giulio Reina
University of Salento
Italy

1. Introduction

For autonomous mobile robots driving across soft soils, such as sand, loose dirt, or snow, it is important to deal with the dynamic effects occurring at the wheel-terrain interface. The most prevalent of these effects are wheel slip and sinkage, which greatly affect a robot's mobility. In general, a vehicle traversing loose sand might experience substantial slip and sinkage, and, hence, poor mobility (see Fig. 1). Conversely, a robot traversing firm clay might undergo small slip and sinkage, and better mobility. As a notable example, field trials performed at the Jet Propulsion Lab (JPL), using a terrestrial analog of the Mars Exploration Rovers have confirmed that there is a great amount of slippage in the drive wheels during traversal of Mars-like terrain (Lindemann & Voorhees, 2005).

Nevertheless, conventional control and localization algorithms generally do not consider the physical characteristics of the vehicle and of its environment. Failure to understand these characteristics could lead to poor position estimation, poor traction, and possibly even to complete immobility. Specifically, the presence of wheel slip precludes the use of conventional dead-reckoning techniques for navigation (Baumgartner et al., 1992; Fuke & Krotkov, 1996; Ojeda et al., 2004), since they are based on the assumption that wheel revolutions can be translated into linear displacement relative to the ground. If one wheel slips, then the associated encoder will register wheel revolutions even though these revolutions do not correspond to a linear displacement of the wheel. Conversely, if one wheel skids, fewer encoder pulses will be produced. Additionally, in presence of side forces, the robot also experiences lateral slip that results in a gradual deviation of the vehicle from the intended path, and possibly in directional instabilities. Minimizing longitudinal and lateral slippage not only limits odometric errors but also reduces the overall energy consumption, and increases the robot's traction and climbing performance.

Wheel sinkage is also a key variable in estimating vehicle-terrain interaction. Wheels can sink in soft soils to depths sufficient to prohibit further motion. Sinkage measurements are as well as valuable for reducing position estimation errors. The accuracy of kinematic models used to estimate rover position updates depends on precise knowledge of the wheel radius, which is used to compute the equivalent linear distance travelled by a wheel from the encoder reading. As the load-bearing strength of soil varies, so does the amount of sinkage and the wheel effective rolling radius, thus decreasing the odometric accuracy.

To reduce the effect of propagating this non-systematic error during rover traverses on varied terrain, a means to measure wheel sinkage (and therefore effective wheel radius) is necessary. In addition, wheel sinkage has been shown to be an important input to terrain identification according to classical terramechanics theory (Iagnemma & Dubowsky, 2004). In summary, it is generally desirable to have the capability to sense excessive wheel slippage and sinkage so that corrective controls may be executed before the vehicle becomes immobile. In turn, the knowledge of the extent of wheel slip and sinkage can improve the accuracy of odometry-based localization system and provide important information about terrain properties.

Fig. 1. Significant wheel slip and sinkage of the rover Dune, constructed at the University of Salento

In this chapter, methods for wheel slippage and sinkage detection are described, aimed to improve vehicle mobility on soft deformable terrain. In detail, a set of indicators to detect longitudinal slippage is described, based on the observation of purely proprioceptive sensors, such as wheel encoders, inertial measurement unit (IMU), and electrical current sensors. A novel approach for lateral slip estimation is also presented, which uses a rearward-facing video camera to measure the pose of the trace that is produced on the ground by the wheels, and to detect whether the robot follows the desired path or deviates from it because of slippage. Since this approach is based on Hough transform supported by Fuzzy logic to provide robust and accurate tracking of the wheel Trace, it is named "FTrace". Finally, an algorithm for visual estimation of wheel sinkage is discussed. It assumes the presence of a monocular camera mounted to the wheel assembly, with a field of view containing the wheel-terrain interface. An artificial pattern, composed of concentric circumferences equally spaced apart on a white background, is attached to the wheel side in order to determine the contact angle with the terrain, following an edge detection strategy. Test results are presented showing the performance of the proposed methods to estimate wheel slippage and sinkage of rover-type robots moving across uneven terrain.

2.1 Related Work
Longitudinal slip can be estimated through the use of encoders by comparing the speed of driven wheels to that of undriven wheels on asphalt (Gustafsson, 1997); however this is not

suitable for deformable surfaces and does not apply for all-wheel drive vehicles or those without redundant encoders. Recent research has investigated the use of either exteroceptive or absolute sensors, or both. Helmick et al., 2006, proposed a system for detecting slippage in a Mars rover based on fusing visual odometry and inertial measurements through a Kalman filter pose estimator. Baumgartner et al., 2001, utilized a sun sensor to improve rover state estimates. Combination of visual odometry with an absolute heading sensor, such as a compass or sun sensor, was shown to be effective for robust long-range navigation (Olson et al., 2001). In contrast to these methods, the approach described in this chapter for longitudinal slip detection relies on purely proprioceptive sensors.

In presence of side forces, the robot moves at an angle (i.e. the slip angle) with respect to its longitudinal axis, resulting in lateral slip as well. A large body of research work exists in the automotive community related to traction control, anti-lock braking systems (ABS), and electronic stability program (ESP). However, these works generally apply to asphalt roads and at significantly higher speeds than those typical for autonomous robots (Robert Bosch GmbH, 2007).

In principle, lateral drift can be estimated using visual motion estimation. It is possible to refer generally to two broad categories: landmark-based and optic flow-based methods. The former methods recognize either natural or artificial landmarks in the environment and, then, infer the position of the robot, usually, by triangulation. The latter approaches estimate the differential of successive images extracting optical flow vectors, which allow changes in the robot pose to be evaluated. Notable examples of this category include visual odometry methods, which were developed and demonstrated for rough-terrain robots (Konolige et al., 2007), and planetary rovers (Maimone et al., 2007). The purpose of visual odometry is that of incrementally estimating the motion of a mobile robot, by detecting and tracking interesting point-features of the environment over subsequent images, generally within a statistical framework for estimation. In some cases, the search for good features to track may be optimized selecting features on specific parts of the scene. Interestingly, point-features extracted from wheel tracks were used by the Mars exploration rover Opportunity for successful visual odometry on piles of sand at Meridiani Planum (see Section 5.1 in (Maimone et al., 2007)). In this regard, the FTrace system represents a different approach. The similarities and differences with respect to existing literature can be summarized in the following points

- It does not use optical flow or estimate incremental motion,
- it estimates the actual travel direction of the robot, i.e. the slip angle,
- it performs landmark tracking; however the FTrace system does not use natural or artificial landmarks in a conventional sense, but it looks at the traces of the vehicle, which can be considered as special landmarks, generated by the vehicle itself,
- trace tracking is performed using a Hough transform detector within a fuzzy inference model.

Previous research in the field of sinkage estimation has measured the change in an articulated suspension's configuration for the purposes of improving odometry and determining the sinkage of wheels relative to one another (Wilcox, 1994). However, absolute sinkage is necessary for mobility analysis and terrain identification algorithms. Potentially, wheel sinkage can be estimated using visual odometry methods (Olson et al., 2001). Practical implementation of these methods may be relatively complex since they rely on the use of

feature identification and tracking algorithms. Brooks et al., 2006 also proposed an online visual sinkage estimation algorithm that relies on the analysis of greyscale intensity along the wheel rim. Assuming that the wheel has a different colour than the terrain, the location of the terrain interface is computed as the point of maximum change in intensity. This method is relatively simple and computationally efficient, but it is sensitive to lighting variations and shadows. Moreover, it is based on the assumption that the wheel has a different grey level than the terrain, which implies previous knowledge of the soil appearance characteristics. Conversely, the proposed method does not require any a priori information about the environment, while preserving computational efficiency.

2. Longitudinal Slip

The greatest enemy of odometric accuracy is wheel-slippage, and vehicles that travel on sandy soils are at risk the most. This is particularly true for rover-like vehicles due to their overconstrained nature, i.e., having more independent motors than degrees of freedom of motion. For these vehicles, any momentary mismatch between wheel velocities with respect to the vehicle kinematic constraints will result in wheels "fighting" each other, and, consequently, slippage with ill-effects such as position estimation errors, increased power consumption, and loss of traction.

In order to detect longitudinal Wheel Slippage (WS), a set of so-called "WS indicators" was developed in (Reina et al., 2006). The general approach is based on observing many different on-board sensor modalities and defining deterministic conditions for wheel slippage. The output of a WS indicator can be a binary flag that indicates that WS has occurred, or it can be a fuzzy quantity that expresses our certainty that WS occurred. Fuzzified outputs from multiple indicators can be combined through fuzzy logic. The most effective WS indicators are:

- *Encoder Indicator* (EI): compares encoder readings with each other.
- *Gyro Indicator* (GI): compares encoder readings with those of the *z*-axis gyro.
- *Current Indicator* (CI): monitors motor currents, which are roughly proportional to the external torque applied to each wheel.

In the remainder of this section, each indicator is discussed in some detail showing experimental results.

2.1 Encoder Indicator

Figure 2 shows a schematic diagram of a six-wheel rover. A coordinate system is attached to the vehicle so that the *y*-axis of the vehicle coordinate system is aligned with the vehicle's longitudinal direction. Each wheel *i,j* has a linear velocity vector $V_{i,j}$ and a steering angle $\varphi_{i,j}$ (index *i* = Front, Center, or Rear, and index *j* = left or right). $\varphi_{i,j}$ is measured between the longitudinal direction of the vehicle Y_b and the steering direction of the wheel. The projection of the speed vector $V_{i,j}$ onto the y-axis is called "longitudinal velocity component" $V'_{i,j}$. While the linear velocities of the wheels differ from each other according to their distance from the Instantaneous Center of Rotation (ICR) of the vehicle, their longitudinal components must be equal on either side of the vehicle.

The underlying hypothesis is that unequal longitudinal velocity components in the three
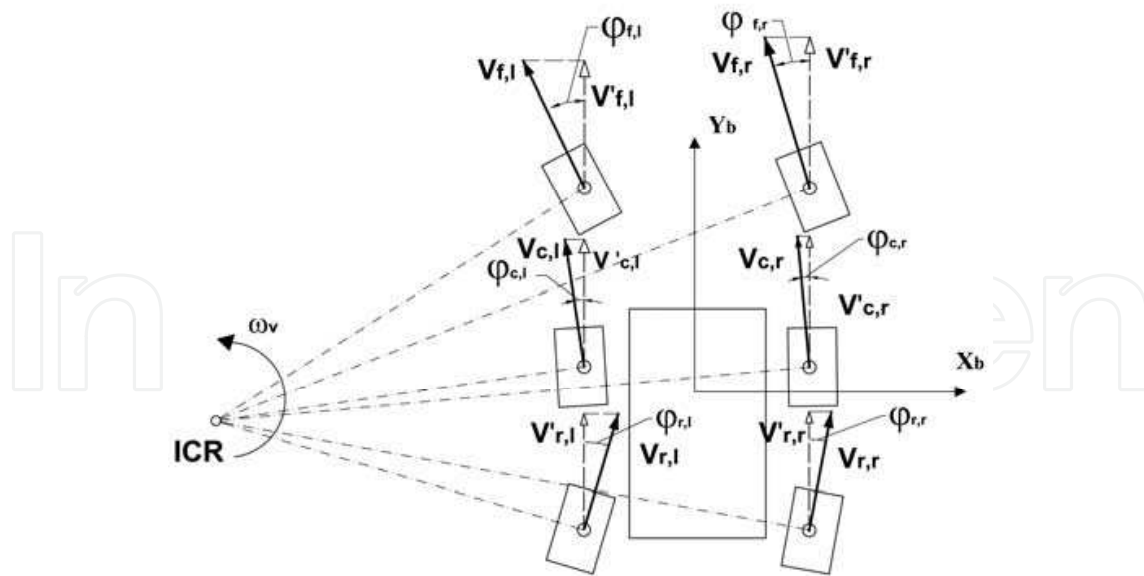
Fig. 2. Nomenclature for wheel velocities in a six-wheel rover

wheels of a side suggest wheel slippage. In order to express this hypothesis, fuzzy logic can be adopted. Details of the fuzzy inference engine can be found in (Reina et al., 2006). The fuzzy data fusion uses three inputs and one output. Inputs are the sensory data, i.e., the differences in longitudinal velocity components between the front and the center wheel, the front and the rear wheel, and the center and the rear wheel, respectively. The output is a dimensionless factor ranging from zero to one that expresses the degree of confidence we have that WS has occurred.

As an example, Fig. 3 shows the output of the fuzzy logic system of the EI for (a) a high-traction and (b) a high-slippage terrain.


(a)   (b)
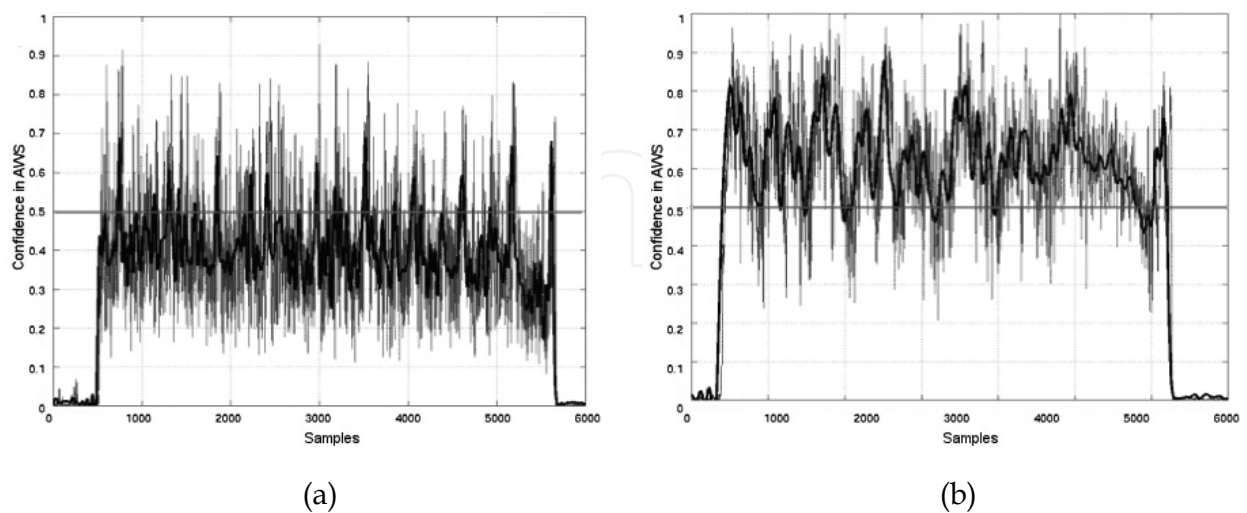
Fig. 3. Output of the Encoder Indicator for different terrains (gray line). The bold black line shows the smoothed output. a) High-traction terrain, no slippage. b) Sloped, sandy terrain causing lots of slippage

2.2 Gyro Indicator

This method aims to detect wheel slippage by comparing encoder data with gyro data. The motion of a rigid body can always be expressed as a momentary pure rotation about the ICR. For straight-line motion, the distance from the ICR to each wheel is of infinite length. The rate-of-turn ω of the vehicle can be computed from each one of the encoder pair i (index i = front, center, and rear), according to:

$$\omega_{Enc,\ i} = \frac{d_{i,r} \cdot \cos\varphi_{i,r} - d_{i,l} \cdot \cos\varphi_{i,l}}{b \cdot T} \tag{1}$$

Where:
$d_{i,\ r/l}$ - distance traveled by the right/left wheel of wheel pair i;
$\varphi_{i,\ r/l}$ - steering angle of the right/left wheel of wheel pair i;
b - vehicle width (distance between the left and right wheel) ;
T - sampling interval.

Each of the three $\omega_{Enc,i}$ can be compared with the rate-of-turn measured by the z-axis gyro ω_{Gyro}, which we consider the ground truth in this approach. If no slippage occurred in a wheel pair, then one can expect good correspondence between the rate-of-turn derived from the encoders of that wheel pair and the gyro. Poor correspondence suggests wheel slippage. Also for the Gyro Indicator, a fuzzy inference system to fuse sensory data was developed (Reina et al., 2006). Figure 4 shows the output of the fuzzy logic system of the Gyro Indicator for a test where the rover was commanded to travel with a constant rate-of-turn of 4°/s on sand. During the run, the wheels were deliberately forced to slip by manually holding back the vehicle using strings attached to its frame. The bold black line is the ground truth, provided by the gyro. The black, dotted grey, and grey lines are the rates-of-turn estimated by the front, centre, and rear encoder pairs, respectively. The output of the GI is expressed in terms of a binary state, which we refer to as an "WS flag" The WS flag is raised whenever the system's confidence in the existence of an WS condition, as estimated by the fuzzy fusion system, is greater than 0.5. This is shown by a grey line in the bottom part of Fig. 4.
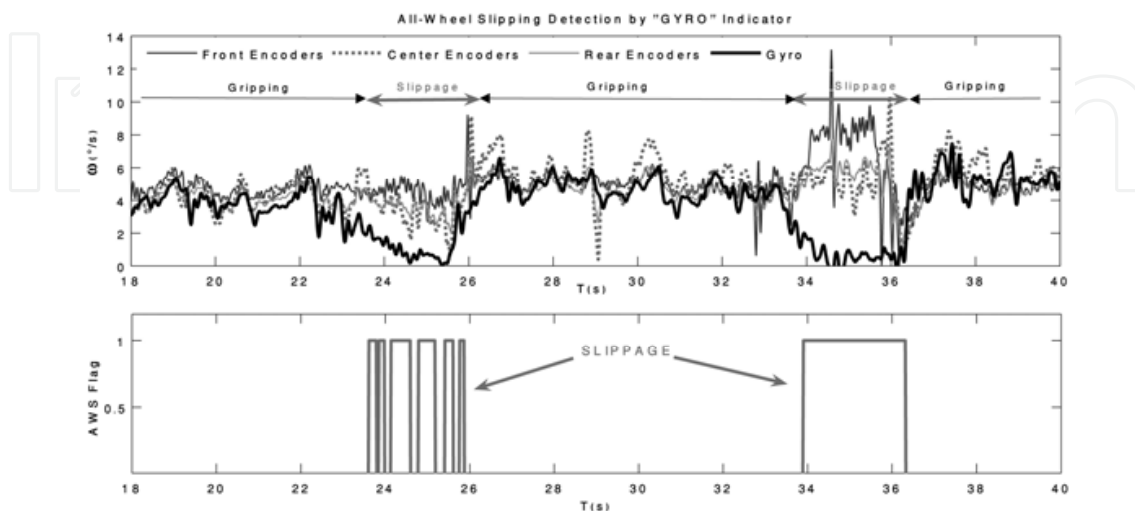

Fig. 4. Effectiveness of the Gyro Indicator

2.3 Current Indicator

The Current Indicator detects WS through the use of the well-established physical model of wheel-terrain interaction mechanics. The interaction between wheel and terrain has been shown to play a critical role in rough terrain mobility (Bekker, 1969). When a torque is applied to the wheel, shearing action is initiated at the wheel-terrain interface creating a force F, which is used to propel the vehicle and overcome the rolling resistance (see Fig. 5). F is usually referred to as the "tractive effort." The maximum tractive effort that can be developed by a wheel is determined by the shear strength of the terrain according to the Coulomb-Mohr soil failure criterion:

$$F_{Max} = A \cdot (c + \sigma \cdot \tan \varphi) = A \cdot c + W \cdot \tan \varphi \qquad (2)$$

where:

c, φ - cohesion and internal friction angle, respectively. These coefficients characterize the behaviour of the terrain;

A - wheel contact patch, which is a function of wheel geometry and of the vertical load acting on the wheel;

σ - normal component of the stress region at the wheel-terrain interface (Fig. 5);

W - vertical load acting on the wheel.

Since torque is proportional to current, the knowledge of the maximum allowable shear strength of a given terrain allows estimation of the electrical current, I_{max}, that is drawn by the wheel drive motor corresponding to the maximum tractive effort. This current is so-called the "*maximum traction current.*" In practice, I_{max} can be determined experimentally for a given terrain, and the condition of total slippage (100%) of the wheel is evaluated as:

$$\left| I_{max} - I_i \right| \leq \Delta I \qquad (3)$$

where I_i is the current drawn by the motor of wheel i and ΔI is an empirically-determined threshold (in our system: 10% of I_{max}). One should note that I_{max} is a function of the vertical load acting on the wheel for a given terrain. For example, when the vehicle is traversing a slope, I_{max} will decrease since less of its weight acts as a force normal to the surface. This is accounted for by increasing ΔI (thus lowering the current threshold that suggests slippage) by an empirically determined factor C_θ. Therefore, (3) can be rewritten as:

$$\left| I_{max} - I_i \right| \leq \Delta I + C_\theta \cdot \theta_r \qquad (4)$$

where θ_r is the rover's pitch angle as measured by the onboard IMU. It should be noted that (4) could only be used for predicting the maximum tractive effort for a wheel. However, methods for evaluating quantitatively the amount of slippage and thus compensating for position estimation errors have been proposed by Ojeda et al., 2006 where a relationship between the electrical currents and wheel slip was obtained to adjust corrupted encoder readings. Errors were reduced well under 1% of the total travel distance and by up to one order of magnitude when compared to conventional dead-reckoning.
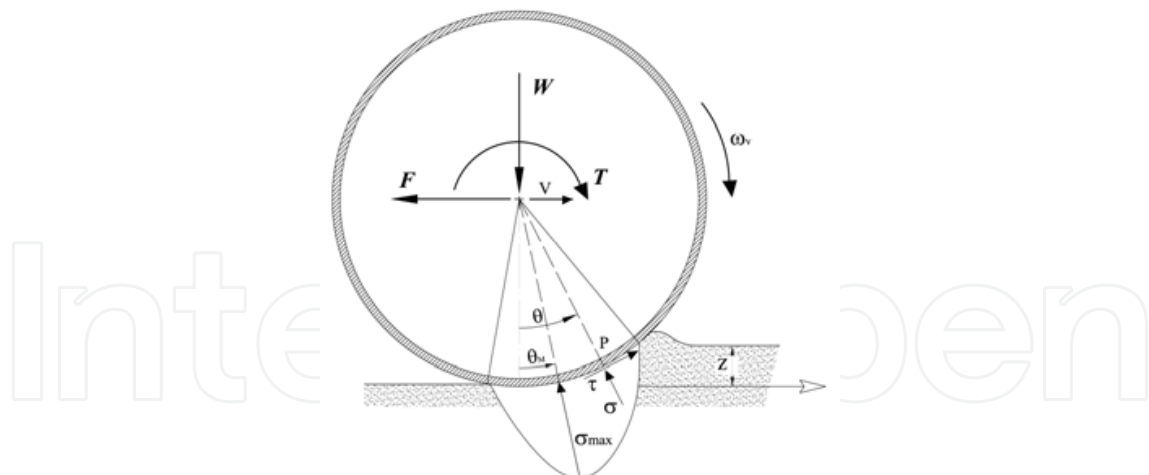
Fig. 5. Wheel-soil interaction model (adapted from (Bekker, 1969)).

2.4 Experimental Results

In this section, experimental results are presented to validate the proposed approach. The effectiveness of the WS indicators was tested on a rover operating in a laboratory sandbox. In this experiment, the robot was commanded to follow a 4-meter straight traversing two consecutive sandy mounds (as shown in Fig. 6), resulting in alternating and varying episodes of slippage. The height of the mounds was about 20 cm.

The slippage detection based on the WS indicators is expressed in terms of a binary output in the form of what we call the WS flag. When the slippage condition established by the indicator is simultaneously met by all the wheels of the vehicle, then the WS flag is raised. The WS flag is lowered when at least one wheel of the vehicle is "gripping." It should be noted that on each of the four corner of the sandbox, an ultrasonic receiver was installed. Together with a star-like formation of four ultrasonic transmitters mounted on the rover, they form a ground truth position measuring system. Within the confined area of our sandbox this system provides absolute position information in real-time and with sub-centimeter accuracy (ground truth).
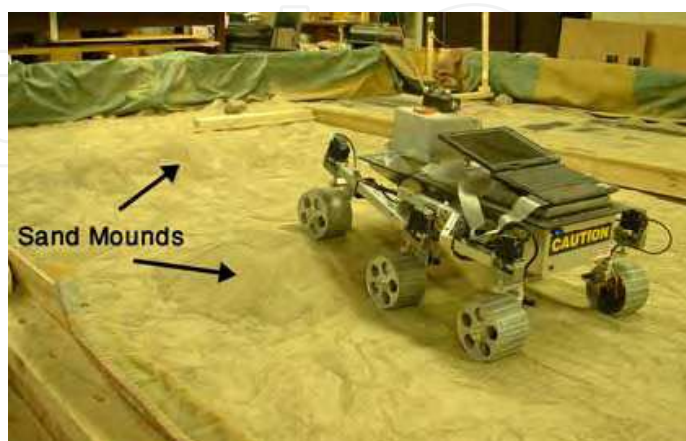

Fig. 6. The rover negotiates a sand mound along a 4-meter path at the Mobile Robotics Laboratory of the University of Michigan
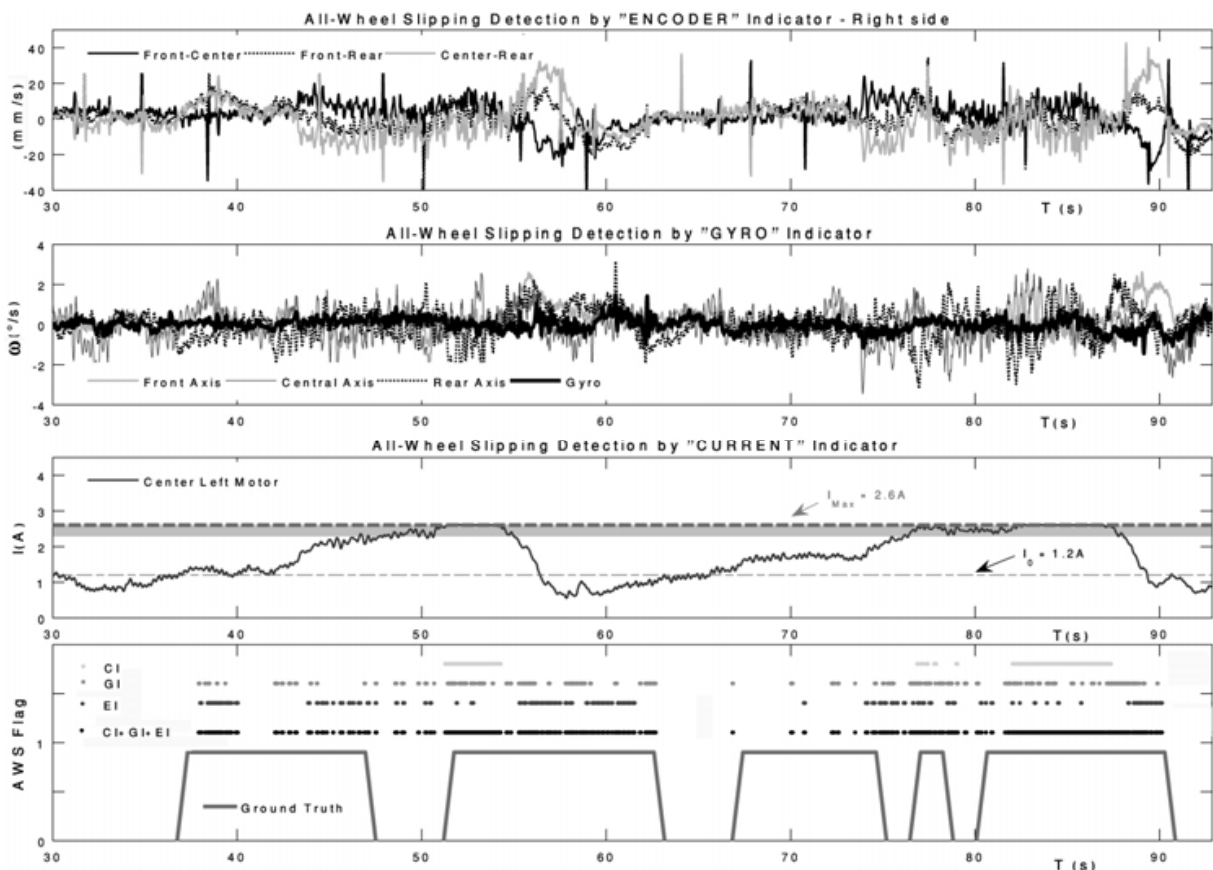
Fig. 7. Effectiveness of the EI, the GI, and the CI during the negotiation of 4-meter path with two sand mounds

The original sensor signals and the output of the indicators are plotted in Fig. 7. The upper plot shows the sensor signals used in the Encoder Indicator for the right side of the vehicle. The black, dotted black, and gray lines are the differences in longitudinal speed between, respectively, the front and the center, the front and the rear, and the center and the rear wheel. The output of the EI is the AWS flag shown by black dots in the bottom graph of Fig. 7. The second plot shows the sensor signals in the GI. Again, the bold black line is the ground truth for this indicator, provided by the gyro.

The gray, dark gray, and dotted black lines are the rates-of-turn as computed by the front, center, and rear encoder pairs, respectively. The output of the GI is the WS flag shown by dark gray dots in the bottom graph of Fig. 7. The third plot shows the electrical current measured in the center left motor. When the slippage condition expressed by (4) is met for all the wheels, then the current-based WS flag is raised. This flag is shown as the gray dots in the bottom graph. We can compare the accuracy of the EI, the GI and the CI WS flags can be compared to the ground truth flag, shown by a continuous gray line in the bottom part of Fig. 7. For this experiment, we found that the EI was correct for 25% of the time whereas the GI flagged WS correctly 38% of the time. The CI flagged WS correctly only 18% of the time. When the three flags were logically OR-ed, the indicators were correct 61% of the time.

3. Lateral Slip

A novel approach for slip angle estimation of mobile robots travelling on loose terrain was presented in (Reina et al., 2010). It uses a rearward-facing video camera to measure the pose of the trace that is produced by the wheels, and detect whether the robot follows the desired path or deviates from it because of slippage. Figure 8 shows a direct example that will help to clarify this method. Figure 8(a) shows a four-wheel rover as driving up a sandy slope following a planned straight path without any significant sideslip. This is shown by two distinct traces parallel to the direction of motion and produced by the wheel pair of either side of the robot. However, if a transverse inclination of the terrain is also present, the consequent external side force acting on rover's body will result in a substantial lateral drift, as shown in Fig. 8(b). The traces, left by the wheels of the same side of the robot, are no longer superimposed and, more importantly, their angle of inclination, with respect to a reference frame attached to the vehicle, differs from the case of absence of slip. The proposed approach aims at estimating the slip angle of the robot by measuring the pose of one of the wheel traces, i.e. the rear left wheel, in conjunction with the knowledge of the rate-of-turn provided by an onboard sensor.

3.1 The FTrace system

The presence of shadows, occlusions, and terrain unevenness can turn trace tracking into a very complex problem. A robust and efficient trace detection system must be able to filter out all disturbances and extract the marking of interest from a non-uniform background. In Fig. 9, a sample image set demonstrates the variety of terrain and environmental conditions that can be encountered. Fig. 9 (a) shows a scene where trace detection can be considered relatively easy thanks to the clearly defined imprint and uniform terrain texture. In Fig. 9 (b), extraction of wheel trace is more difficult due to the presence of terrain discontinuities, whereas Fig. 9 (c) shows a non-uniform terrain texture. A more complex wheel trace is shown in Fig. 9 (d) and Fig. 9 (e), due to the presence of heavy shadowing. Finally, Fig. 9 (f) refers to a condition where two imprints are present in the same scene.

(a)   (b)
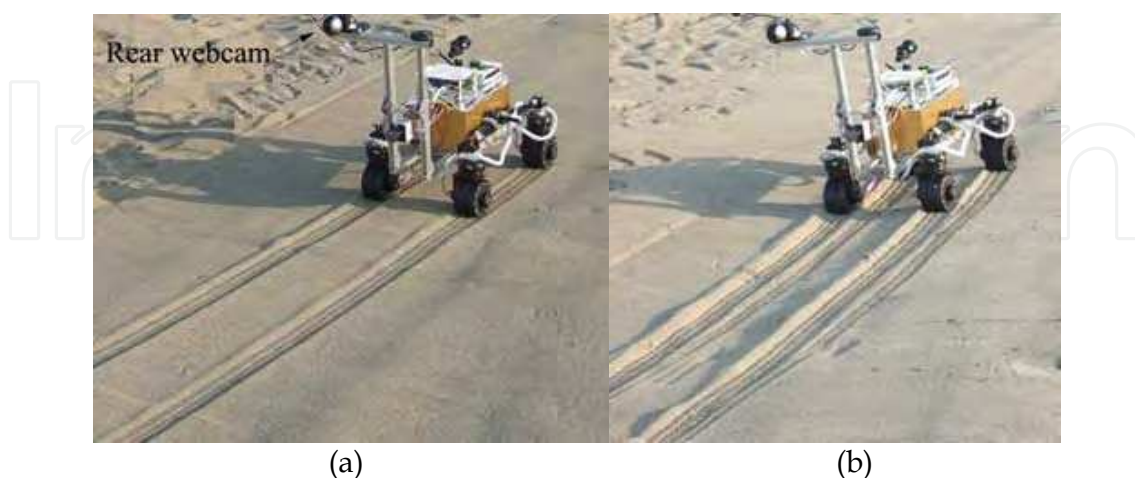
Fig. 8. Sideslip estimation for the robot El-Dorado, built at the Space robotics Lab of Tohoku University, by visual observation of the wheel traces with a rear webcam: (a) wheel traces parallel to the direction of motion, no lateral slip, (b) wheel traces inclined with respect to the intended direction of motion, significant lateral slip.
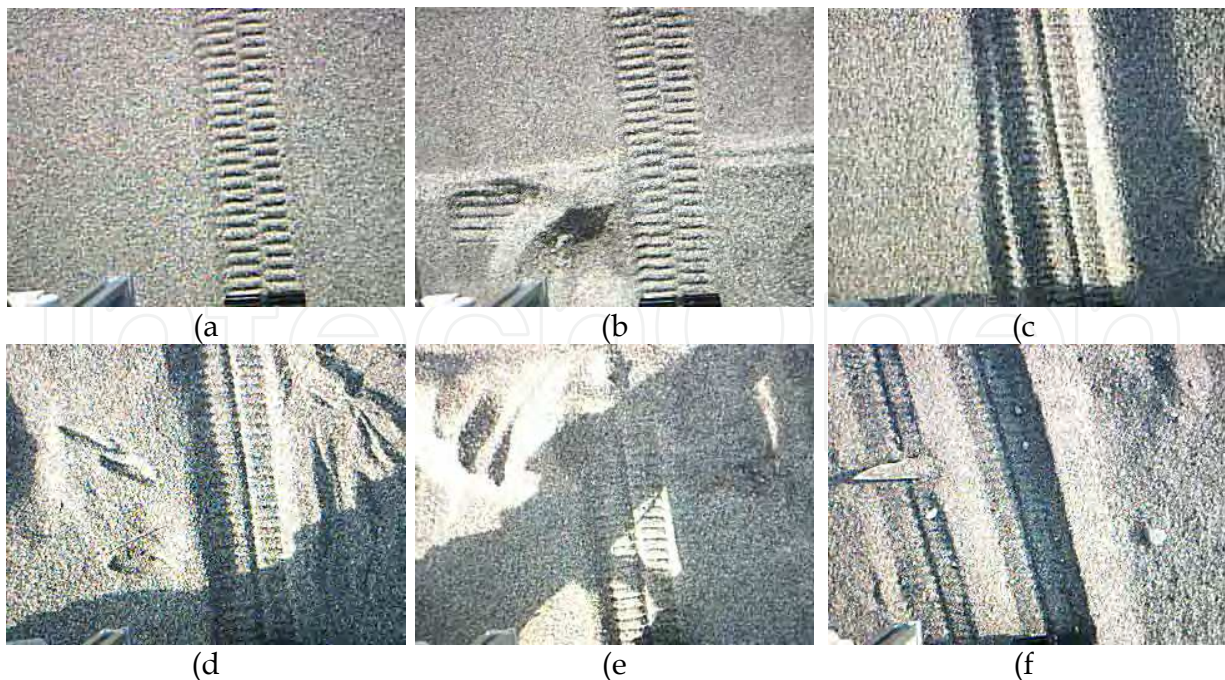
Fig. 9. Sample images of terrain and wheel trace conditions: (a) uniform sandy terrain, (b) disturbances due to transversal line-like discontinuities, (c) non-uniform terrain texture, (d) and (e) non-uniform terrain texture with noise due to shadowing, (f) different trails present in the scene.

The FTrace module performs two main tasks. For more details, the reader is referred to (Reina & Yoshida, 2008):

- Extraction of trace candidates from the camera-acquired image and estimation of their pose with respect to the sensor, i.e. the vehicle, reference frame.
- Selection of the candidate that best fits to the trace model.

In order to determine which line best fits to the trace model, the system employs a robust Hough transform enhanced by fuzzy reasoning. The general approach is based on comparing the geometrical properties of each candidate with those of the trace model in both the image plane of the camera and the real world, and defining deterministic conditions for model matching. The output of the FTrace is a fuzzy quantity that expresses the certainty that the line agrees exactly with the trace model. As a representative result, Figure 10 shows a sample image referring to a field trial on sandy terrain. The FTrace system was able to extract ten candidates from the original scene (Fig. 10(a)), as shown in Fig. 10(b) and Fig. 10(c). The trace selection stage provided the confidence matches collected in Table 1. The lane marker, denoted with L_5 in Fig. 10(b) and shown by a dotted line in Fig. 10(c), yielded the greatest confidence level (89.0%), and was therefore selected as the best match. In Fig. 10(d), the output of the FTrace system is overlaid over the original image along with the estimated values of lateral slip.

3.1 Field Validation
In this section experimental results are presented, aimed at validating our approach for lateral slip estimation by visual observation of the wheel trace.

(a)   (b)

(c)   (d)
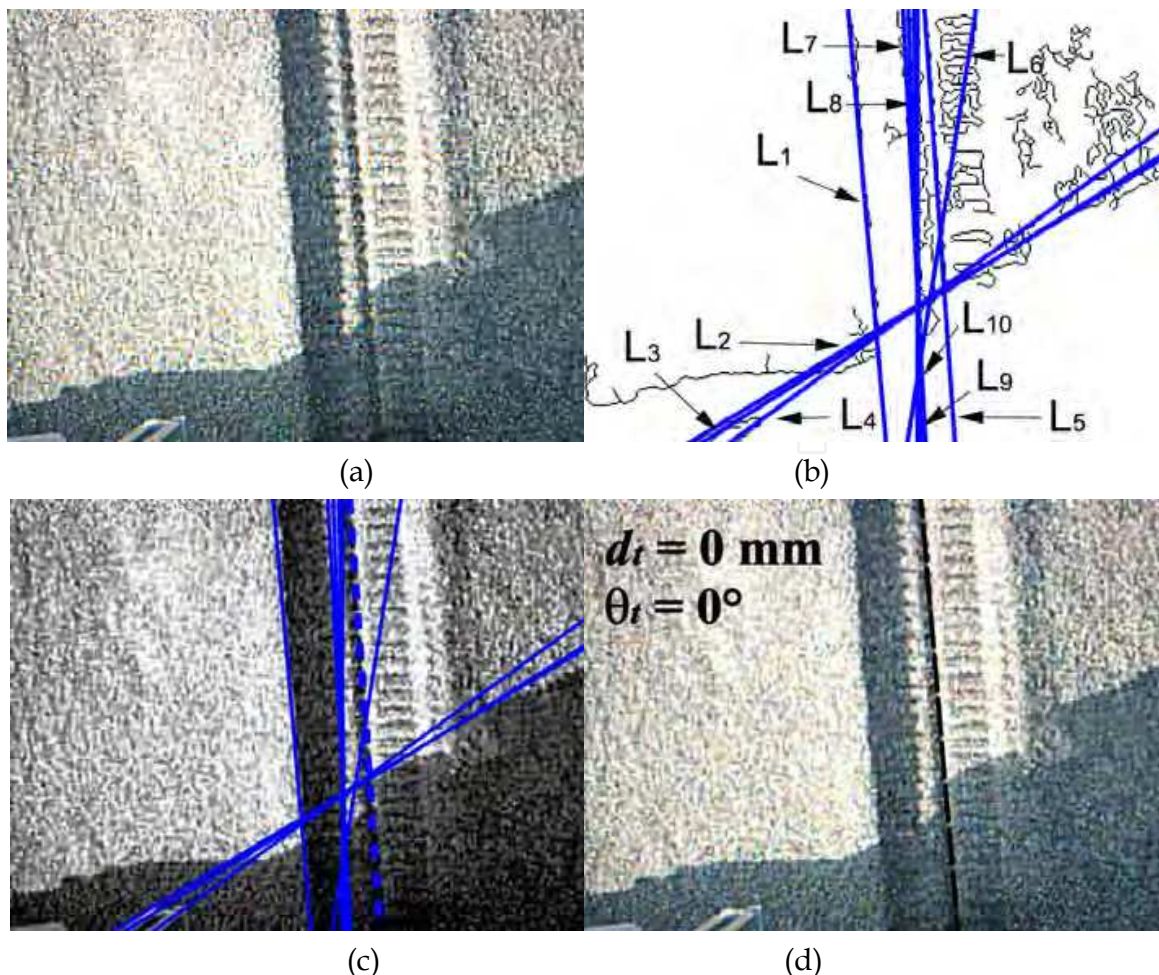
Fig. 10. Application of the FTrace system to a sample image: a) original scene, b) and c) application of edge detection and Hough transform, d) output of the FTrace system. Note that for this image no sideslip was detected.

The FTrace system was tested in the field using a four-wheel rover, outfitted with a cost-effective webcam acquiring at 5 Hz and with a field of view on the ground corresponding to a 60 cm long × 80 cm wide area, behind the left rear wheel. The test field was located on the shoreline of a sandy beach, comprising large flat areas and sparse mounds of different extensions and heights. In all experiments, the rover was remotely controlled using a wireless joypad, and commanded to follow a straight-line path with a travel speed of about 8 cm/s. Two types of environment were considered:

- Set A: sandy relatively flat terrain. These experiments were aimed at evaluating undue errors of the FTrace system incurred by low-slippage terrain.
- Set B: sandy non-flat terrain, including driving uphill or sideways on sandy slopes with substantial lateral slip.

The entire experimental area was within the distance range (order of tens of meters) of a laser-based absolute positioning system that provided the ground-truth.

The FTrace system was tested over a total of 15,016 images (about 250 m of overall travel distance) showing the results collected in Table 2 for both sets of experiments. The percentage of false positives, i.e. a trace marker detected when actually there is no trace

marker, was less than 0.3%, and limited to the initial moments of robot's motion, when no wheel track was present on the ground yet. Note that in the initial stage, the FTrace system relies only on Hough transform to extract strong lines from the scene, which pass through the wheel centre, whereas the fuzzy inference system kicks in after the rover begins travelling. Conversely, false negatives arise when the trace marker is present in the image but the system is not able to detect it at all and does not return any information.

SET#	Frames	False Positives (%)	False Negatives (%)	Misid. (%)
A	2560	0.1	1.5	0.0
B	12456	0.2	2.7	0.8

Table 1. Results obtained from the FTrace system for different types of terrain. Set A: flat sandy terrain. Set B: non-flat sandy terrain

Candidate Line #	L_1	L_2	L_3	L_4	L_5	L_6	L_7	L_8	L_9	L_{10}
Confidence Match (%)	4.1	1.1	1.3	1.4	89.0	9.1	20.0	20.3	18.7	20.2

Table 2. Degree of confidence in model matching for the wheel trace candidates of Fig. 10, as derived from the FTrace system.

The percentage of false negatives was less than 3%, and due largely to poor image segmentation and camera calibration errors (80%), and model approximation (20%). In those cases the last detected wheel trace is retained for comparison with the successive scenes. This approach proved successfully since the number of consecutive false negatives was always less than 3 (< 0.6 s). Finally, misidentifications refer to cases in which a trace marker is present in the image, but the system fails in recognizing it properly and returns wrong information. In all tests, misidentifications were less than 1%. Overall, the system proved to be robust to disturbances due to heavy shadowing, non-uniform terrain texture, and the presence of overlapping imprints.

The accuracy of the FTrace system in estimating the lateral drift of the robot was assessed in an experiment on non-flat terrain. The rover was driven up an approximately 5-degree sandy slope. During its path, the robot climbed sideways on a large mound, resulting in continuous and almost constant lateral drift. Figure 11 shows the position of the robot and the imprints produced by its wheels at the end of the run, from a front and rear view, respectively. The total travel distance resulted in about $D=7$ m. The slip angle, derived from the FTrace system, is compared with the ground-truth data in Fig. 12. The two curves show good agreement with a root mean square (RMS) error less than 1.5 deg.

The FTrace system detected effectively the onset of sideslip and its successive trend throughout the experiment. Two different stages can be distinguished during the test. In the first stage, referring to the first 60 seconds, the robot followed its intended straight path without any significant drift. This is demonstrated by the two wheel traces parallel to the direction of motion. The second stage marks the onset of sideslip caused by the external

lateral force acting on the rover due to the transverse inclination of the terrain. As a direct consequence, the angle of inclination of the wheel traces changes, (see also Fig. 11(b)), attesting to the feasibility of this approach.

Fig. 11. Position of the rover and wheel traces at the end of the traverse of a sandy slope: a) Front view, b) rear view

In order to allow useful dead-reckoning even in presence of lateral drift, a method for slippage compensated odometry was presented by Reina et al., 2010 using an integrated longitudinal and lateral friction model. This approach was proved to be effective in correcting odometry errors caused by wheel slippage, during traverse of sandy slopes.

As a representative result, Fig. 13 shows the path followed by the robot as estimated from plain odometry by a dash black line, for the previously-described test. The path derived from the slippage-compensated odometry is shown by a solid gray line. Both data can be compared with the ground-truth shown by a solid black line. An absolute radial error E was computed for the estimation of the final position of the robot. The error in the estimation of the final position of the robot using odometry was E_e=2.84 m. If odometry is enhanced by measuring the actual heading of the robot with an onboard compass rather than wheel encoders, the error was decreased to E_{oc}=2.50 m. When using the sComp odometry the final position error was limited to a remarkable E_{sC}=0.14 m with an overall reduction of 95% with respect to plain odometry, and 83% compared to compass-enhanced odometry.

4. Wheel Sinkage

The algorithm aims to measure wheel sinkage in deformable terrain from an image of the wheel. It is assumed that a camera is attached to the wheel assembly with a field of view containing the wheel-terrain interface, and that its location relative to the wheel is known and fixed during vehicle travel. The wheel under inspection needs to be outfitted with a

pattern composed of equally spaced concentric circumferences on a white background, as shown by the practical implementation of the visual sinkage estimation (VSE) system in Fig. 14.(a). Since the wheels of off-road robots are mostly customized, this should not require much effort. Sinkage z can be estimated by measuring the contact angle between wheel and terrain. The algorithm relies on a relatively simple edge-detection approach. The idea is to identify the wheel radial lines, along which the number of edges is less than that expected when the wheel rolls without sinkage. Those lines can be associated with the part of the wheel obscured by terrain and thus with sinkage, as shown in the explanatory scheme of Fig. 14. (b).
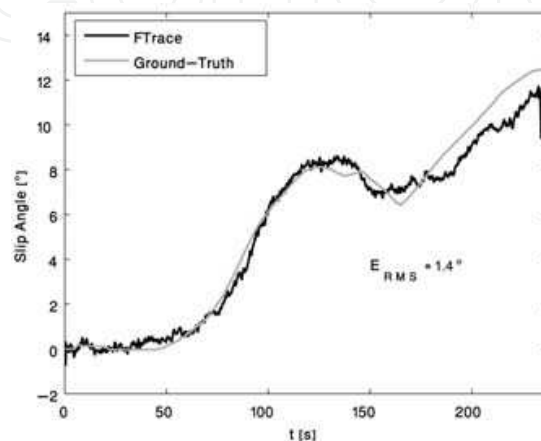
Fig. 12. Effectiveness of the FTrace system in estimating the robot slip angle during sideways traverse of a sandy slope
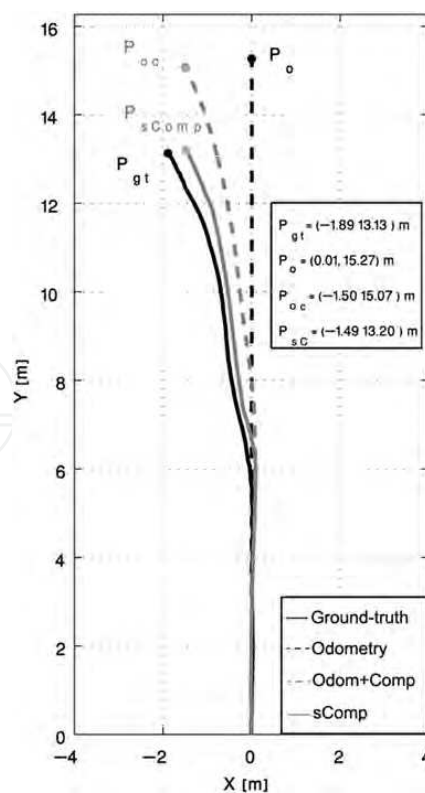
Fig. 13. Position estimation of the rover path during the traverse of a sandy slope

One should note that alternative configurations of this approach may be thought and implemented, using, for example, a belly-mounted camera. This would fix the potential drawback of having an off-side-sensor. To determine the contact angle, only the annular region along the wheel rim and including the pattern needs to be examined. By limiting the analysis only to this region of interest, the accuracy of the algorithm can be improved and its computational burden reduced. More details of the visual algorithm can be found in (Reina et al., 2006).
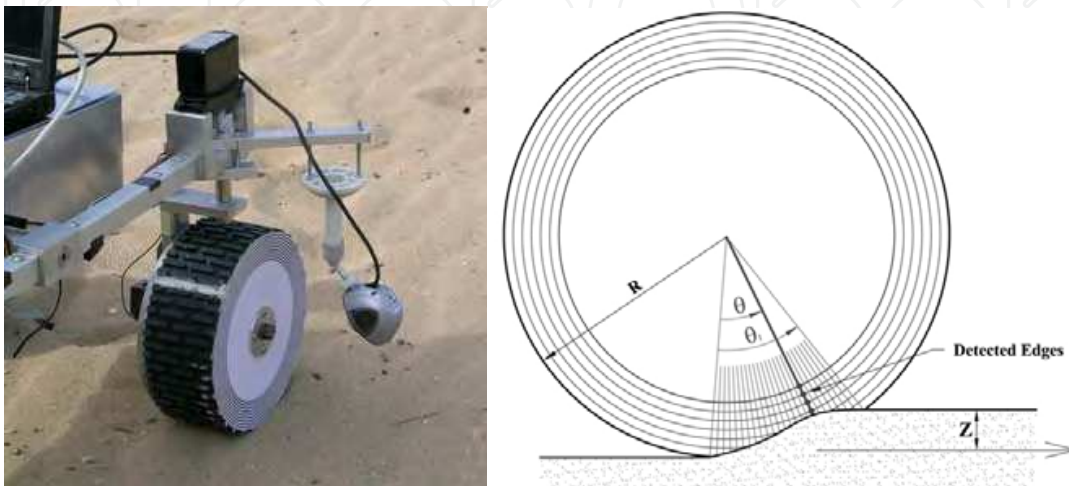
Fig. 14. Robot wheel outfitted for the VSE system (a), strategy for sinkage estimation (b)

The VSE system was validated using a single-wheel test bed. Sinkage was successfully estimated over a total of 31,000 images with a root mean square error of 2.0 mm. the percentage of false positives, that is, sinkage detected when actually there is no wheel sinkage, was less than 0.3%, mostly due to rocks or terrain unevenness occluding the wheel-terrain interface. Conversely, false negatives arise when the wheel experiences sinkage but the system is not able to detect it at all and does not return any information. No false negatives were detected in all the experiments. The algorithm also proved to be very robust against variations of lighting conditions up to lighting reduction as much as 90% of the optimal value.
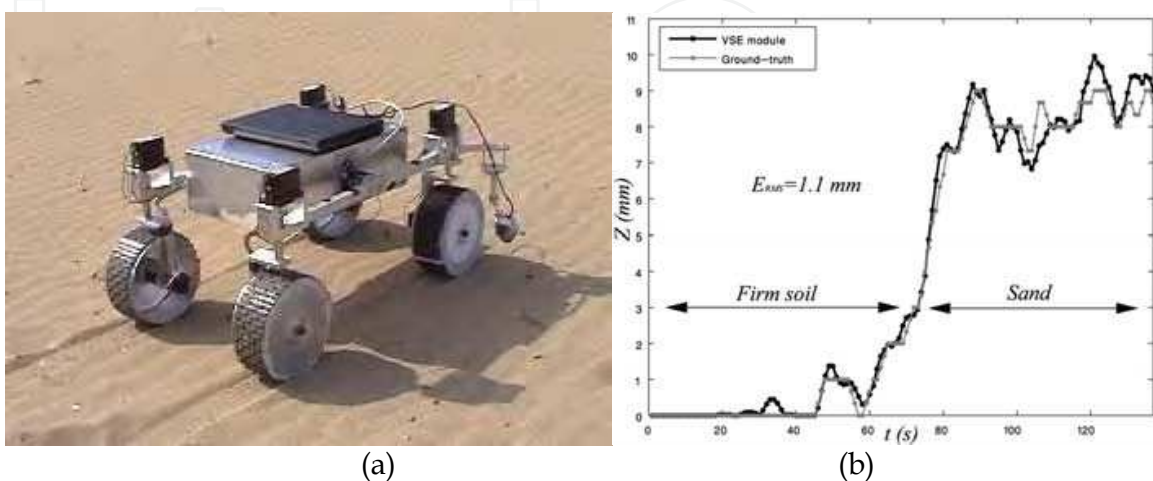

Fig. 15. Sinkage estimation in the field: (a) VSE system integrated with the University of Salento rover Dune, (b) sinkage measurement

The visual algorithm was also tested in the field using an all-terrain rover operating in natural outdoor terrains. The test field was located on the shoreline of a sandy beach (as shown in Fig. 15.(a)), comprising a few areas of firm, rocky terrain. A set of experiments was performed to prove the ability of the rover in detecting changes in the physical properties of the traversed terrain, based on the measure of wheel sinkage. Under the assumption of almost constant vertical load acting on the wheel, sinkage is expected to increase in soft soils than in firm terrains. This on-board capability would enable the rover to adopt proper actions to revise its motion plan and avoid hazardous highly-deformable terrains, or modulate wheel torque to improve traction and limit slippage.

In all experiments, actual values for the wheel sinkage were manually measured by a human analyst, based on the acquired images. Figure 15(b) shows the sinkage as estimated by the VSE module in a representative test, where the rover started its path from firm terrain, and then moved on dry sand with a constant travel speed of 10 cm/s. As expected, sinkage was null during the robot motion on rigid surface, and increased as the vehicle travelled on sandy soil. The vision-based measurement matches very well the ground-truth with a RMS error of 1.1 mm.

5. Conclusions

This chapter discussed methods for wheel slip and sinkage estimation to improve mobility of rough terrain vehicles and planetary rovers. Specifically, novel measures for longitudinal slippage identification were introduced, which compare readings from encoders with each other, with data from a gyroscope, and with current sensors mounted on onboard the vehicle. It was shown that this method was effective in experimental trials on sandy, non-flat terrain. An innovative method for sideslip estimation was presented, based on observing the wheel trail left by a robot during its traverse of loose sandy terrains. Comprehensive experiments in the field demonstrated the overall effectiveness of the proposed approach. The FTrace method was able to measure the slip angle of the robot with a worst-case of less than 3% of failed observations and 1.6 deg of accuracy. Finally, a vision-based algorithm for wheel sinkage estimation was also proposed and shown to be computationally efficient, relatively accurate with maximum errors below 15%, and very robust to disturbances and variations in lighting condition.

These techniques can be used to gain important information about the vehicle-terrain interaction and to improve dead-reckoning accuracy and traction control in rough-terrain autonomous vehicles.

6. References

Baumgartner, E.T., Aghazarian, H., & Trebi-Ollennu, A., (2001). Rover Localization Results for the FIDO Rover, *Proceedings of the Conf. Sensor Fusion and Decentralized Control in Autonomous Robotic Systems*, Vol. 4571, pp. 34-44, Newton, MA, USA.

Bekker, G., (1969). *Introduction to Terrain-Vehicle Systems*, Ann Arbor, University of Michigan Press.

Brooks, C.A., Iagnemma K. & Dubowsky, S., (2006). Visual Wheel Sinkage Measurement for Planetary Rover Mobility Characterization, *Autonomous Robot*, Vol. 21, pp. 55-64.

Fuke, Y., & Krotkov, E., (1996). Dead reckoning for a lunar rover on uneven terrain, *Proceedings of the IEEE Int. Conf. on Robotics and Automation*, Vol. 1, pp. 411-416.

Gustafsson, F., (1997). Slip-based tire-road friction estimation. *Automatica*, Vol. 33(6), pp. 1087-1099.

Helmick, D., et al., (2006). Slip Compensated Path Following for Planetary Exploration Rovers. *Advanced Robotics*, Vol. 20(11), pp. 1257–1280.

Lindemann, R.A. & Voorhees, C.J. (2005). Mars Exploration Rover Mobility Assembly Design, Test, and Performance, Proceedings of the IEEE Conf. Systems, Man, Cybern., Waikoloa, Hi, pp. 450-455.

Iagnemma, K. & Dubowsky, S., (2004). *Mobile Robots in Rough Terrain: Estimation, Motion Planning, and Control with application to Planetary Rovers*. Springer Tracts in Advanced Robotics (STAR) Series, Vol. 12, Springer.

Konolige, K., Agrawal, M., & Sola, J., (2007). Large-Scale Visual Odometry for Rough Terrain, *Proceedings Int. Symposium on Research in Robotics*, Hiroshima , Japan.

Maimone, M., Cheng, Y., and Matthies, L., (2007). Two Years of Visual Odometry on the Mars Exploration rovers, *Journal of Field Robotics*, Vol. 24(3), pp. 169-186.

Olson, C., Matthies, L., Schoppers, M., & Maimone, M. (2001). Stereo ego-motion improvements for robust rover navigation, *Proceedings of the IEEE International Conference on Robotics and Automation*.

Ojeda, L., Reina, G. & Borenstein, J. (2004). Experimental Results from FLEXnav: An Expert Rule-based Dead-reckoning System for Mars Rovers, *Proceedings of IEEE Aerospace Conf.*, Big Sky, MT, USA.

Ojeda, L., Cruz, D., Reina, G. & Borenstein, J. (2006). Current-based slippage detection and odometry correction for mobile robots and planetary rovers. *IEEE Transactions on Robotics*, 22(2), pp. 366-378.

Reina, G., Ojeda, L., Milella, A. & Borenstein, J. (2006). Wheel Slippage and Sinkage Detection for Planetary Rovers. *IEEE/ASME Transactions on Mechatronics*, Vol. 1(2), pp. 185-195.

Reina, G. & Yoshida, K., (2008), Slip Angle Estimation for Lunar and Planetary Robots. *Int. Journal of Intelligence Control and Systems*, Special Issue on Field Robotics, 13(1), pp. 15-24 .

Reina, G., Ishigami, G., Nagatani, K. and Yoshida, K., (2009). Odometry Correction Using Visual Slip-Angle Estimation for Planetary Exploration Rovers, accepted for publication in *Advanced Robotics*, 2010.

Robert Bosch GmbH (2000). *Automotive Handbook*, 5th ed., Germany.

Wilcox B., (1994). Non-geometric hazard detection for a mars microrover, *Proceedings of the AIAA Conf. Intelligent Robotics in Field, Factory, Service, and Space*, Vol. 2, pp. 675-684. Houston, TX, USA.
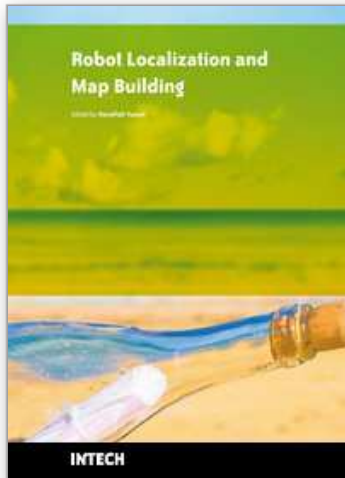
Robot Localization and Map Building

Edited by Hanafiah Yussof

Localization and mapping are the essence of successful navigation in mobile platform technology. Localization is a fundamental task in order to achieve high levels of autonomy in robot navigation and robustness in vehicle positioning. Robot localization and mapping is commonly related to cartography, combining science, technique and computation to build a trajectory map that reality can be modelled in ways that communicate spatial information effectively. This book describes comprehensive introduction, theories and applications related to localization, positioning and map building in mobile robot and autonomous vehicle platforms. It is organized in twenty seven chapters. Each chapter is rich with different degrees of details and approaches, supported by unique and actual resources that make it possible for readers to explore and learn the up to date knowledge in robot navigation technology. Understanding the theory and principles described in this book requires a multidisciplinary background of robotics, nonlinear system, sensor network, network engineering, computer science, physics, etc.

How to reference

In order to correctly reference this scholarly work, feel free to copy and paste the following:

Giulio Reina (2010). Methods for Wheel Slip and Sinkage Estimation in Mobile Robots, Robot Localization and Map Building, Hanafiah Yussof (Ed.), ISBN: 978-953-7619-83-1, InTech, Available from: http://www.intechopen.com/books/robot-localization-and-map-building/methods-for-wheel-slip-and-sinkage-estimation-in-mobile-robots

INTECH
open science | open minds